Electrochimica Acta 429 (2022) 141044

Contents lists available at ScienceDirect

Electrochimica Acta

journal homepage: www.journals.elsevier.com/electrochimica-acta

Anodic TiO_2 nanotube layers decorated by Pd nanoparticles using ALD: An efficient electrocatalyst for methanol oxidation

Bilal Bawab [a], Sitaramanjaneya M. Thalluri [a,b], Jhonatan Rodriguez-Pereira [a,b], Hanna Sopha [a,b], Raul Zazpe [a,b], Jan M. Macak [a,b,*]

[a] Central European Institute of Technology, Brno University of Technology, Purkynova 123, 61200 Brno, Czech Republic
[b] Center of Materials and Nanotechnologies, Faculty of Chemical Technology, University of Pardubice, Nam. Cs. Legii 565, 53002 Pardubice, Czech Republic

ARTICLE INFO

Keywords:
TiO_2 nanotube layers
Pd nanoparticles
Atomic Layer Deposition
Electrocatalysis
Methanol electro-oxidation

ABSTRACT

Herein, we report the performance of Pd nanoparticles (NPs) prepared by Atomic Layer Deposition (ALD) as a catalyst for methanol electro-oxidation. Pd NPs were decorated onto anodic TiO_2 nanotube (TNT) layers as supporting material that possess a large available surface area and direct electrical contact via the underlying titanium foil. Different Pd loadings (150 – 300 – 450 – 600 ALD cycles) show different particles sizes ranging between 7 and 12 nm, as revealed by transmission electron microscopy. Coalescence dominated visibly from 450 ALD cycles, which led to a porous Pd layer all along the TNT walls rather than the growth of individual particles. Electrocatalytic performance was investigated by cyclic voltammetry (CV), where the catalytic activity increased proportional with Pd loading up to the highest values for 400 and 450 cycles, whereas a further increase in the number of ALD cycles (N_{ALD}) did not show any additional improvement in methanol oxidation current densities. TNT layers decorated with 400, 450 and 600 Pd ALD cycles show featureless curves suggesting complete anti-poisoning ability or possibly a proof of a direct conversion from CH_3OH to CO_2 (without any intermediate byproducts). The lack of an oxidation peak during the anodic scan and therefore a reduction peak during the cathodic scan, confirms Pd NPs (stabilized by TiO_2) efficiently utilize OH_{ads} and chemisorbed CH_3OH in a way that its CO poisoning was inhibited. As a result, the tuned high surface area TNT layers exhibited excellent performance as a supporting material for Pd NPs against formation of electrochemical poisoning species. Finally, the mechanism of the TNT layers interaction with Pd NPs, which led to the propelling methanol oxidation reaction without loss in performance over cycling is postulated.

1. Introduction

The ever-increasing global energy demand, along with the environmental issues originated from the use of fossil fuel, triggered an intense search for sustainable and clean energy alternatives. Direct methanol fuel cells (DMFCs), in which the chemical energy stored in methanol is converted to electrical energy, have been explored in the last years. Unlike hydrogen fuel cells, DMFCs use liquid fuel that allows easier handling and transportation. The two main reactions that determine the activity of DMFCs are the anodic methanol oxidation reaction (MOR) and cathodic oxygen reduction reaction (ORR) [1]. The catalytic reaction kinetics during the fuel cell activity is dependent on the electrode surface morphology and/or nanoparticles (NPs) sizes. Larger NPs can relatively increase the NPs surface exposed to the surrounding electrolyte as compared to the interacted substrate surface [2]. In contrary, smaller NPs are less likely to have CO poisoning specially at high temperatures, due to oxygen bond break resulting in oxygen desorption at this level, which shows more resistant to CO poisoning [3]. Noble metal-metal oxide–support interactions generally play a significant role in electrocatalysis, as they maintain a high catalytic activity of noble metal NPs due to their tolerance towards poisoning from reaction byproducts. The use of metal oxide supports, such as MnO_2 [4], SnO_2 [5], or TiO_2 [6], proved to be very beneficial as they are highly stable and maintain consistent conversion efficiency in fuel cells. Supporting materials, decorated by NPs as a catalyst, enhance the electron transport at the catalyst/electrolyte interface. The presence of oxide as a supporting material, whether it is a reducible metal oxide, such as TiO_2 or FeO_x, or a non reducible oxide such as ZrO_2 [7], can directly affect the catalytic activity. For instance, in catalytic converters used in the automotive industry, CO interacts with oxygen on the catalyst surface

* Corresponding author.
E-mail address: jan.macak@upce.cz (J.M. Macak).

https://doi.org/10.1016/j.electacta.2022.141044
Received 20 March 2022; Received in revised form 3 August 2022; Accepted 14 August 2022
Available online 15 August 2022

producing CO_2. Hence, the reaction can proceed in two directions. In case the supporting material provides oxygen, as it happens with TiO_2, these oxygen atoms will substitute the missing oxygen on the surface. Otherwise, CO most likely substitutes oxygen atoms and deactivates the surface [8]. In parallel, approaches based on variations in the electrode morphology (nano-, meso-, and macroporous materials) have shown a huge impact to prevent the development and accumulation of intermediate products on the active electrode surface. In addition, the use of alkaline electrolytes showed higher catalytic activity towards the anodic regime compared with acidic electrolytes [9]. One must bear in mind that testing noble metals, such as Pd, under intense anodic conditions in alkali medium can result in total deactivation, due to the formation of Pd hydroxylates. Also the electrolyte concentrations can directly influence the MOR rate [10].

Regarding the noble metal NPs used as catalyst towards methanol electro-oxidation, the inherent stability of Pt makes it a great catalyst choice as an anode in DMFCs. However, taking into consideration the Pt scarcity and the corresponding high costs for large scale Pt production, a search for alternative catalysts has been initiated. Alloys of Pt with other noble metals, such as Pd, are considered to be used on DMFCs electrodes in order to reduce or substitute Pt mass. While a complete methanol (CH_3OH) oxidation during the electrochemical process involves the transfer of 6 electrons to obtain CO_2 as an end-product, incomplete oxidation can result in other undesired products such as formaldehydes, formic acids, and CO [11]. Pd has the tendency to bond with CO molecules, which leads to poisoning of the active surface. Even at lower temperatures, the process can still facilitate CO to react, forming Pd $(CO)_x$ compounds [12]. Hydration reaction that is more predominant on Pd surface as compared to Pt, can later form OH groups that support the de-poisoning process of the intermediate "CO" during methanol oxidation [13], as shown later in this paper.

The importance of having NPs is based on the fact, that it significantly improves the surface to volume ratio, providing more catalytic active sites. The growth of uniform Pd NPs on high specific surface area supporting materials is of paramount importance due to the improved NPs count per unit area of support, thus increasing the catalytic activity of the process. Several reports were reported on the employment of Pd NPs on different substrates [14–16]. The available literature shows that the deposition of Pd NPs on TNT layers utilizing different techniques such as electrochemical milling [17], chemical bath deposition [18,19] and electrodeposition [20], suffers from non-uniform depositions with variations in coverage density all along the surface. Some of the published literatures have focused on ALD based deposition of Pd NPs on TNT layers for their applications on organic molecule degradation [2,15, 21,22]. Well dispersed Pd NPs over TNT layers were obtained in these papers and their activities for different catalytic reactions were proposed. However, TNT layers as a standalone are not a good material for the electrocatalytics purposes, knowing its poor electrical conductivity. However, as a supporting material, high surface area TNT layers can be detrimental to facilitate the oxidation of reactant molecules (methanol). This is due to an enormous amount of surface hydroxyl groups that are well known to oxidize intermediate products, majorly CO generated during methanol electrooxidation [23].

The aim of the current study is to conformaly decorate TNT layers by homogeneously distributed Pd NPs using ALD and to evaluate their catalytic activity profiles for methanol electro-oxidation. Therefore, the ability of Pd NPs on TNT (Pd/TNT) layer electrodes to withstand against surface poisoning is elaborated. Pd NPs were decorated by ALD onto 5 μm thick anatase TNT layers. The morphology and the chemical composition of the resulting Pd/TNT layers were investigated in detail by scanning electron microscope (SEM), transmission electron microscope (TEM), X-ray diffraction (XRD), and X-ray photoelectron spectroscopy (XPS). The electrocatalytic activity of Pd/TNT layers towards methanol electro-oxidation was evaluated by cyclic voltammetry (CV) and chronoamperometry (CA) as a function of the number of ALD cycles.

2. Experimental part

2.1. TNT layer preparation

The detailed protocol for the TNT layer was published in our previous work [24]. Briefly, Ti foils (Sigma-Aldrich, 0.127 mm, 99.7% purity) were degreased and anodized at room temperature using a high-voltage potentiostat (PGU-200 V, IPS Elektroniklabor GmbH) to develop TNT layers of ~5 μm thickness and ~230 nm diameter in an ethylene glycol-based electrolyte containing 10% water and 0.15 M NH_4F at 100 V for 4 hours. Ti foils and TNT layers were annealed in air for 1 h at 400 °C.

2.2. Atomic layer deposition of Pd

Pd NPs were deposited onto TNT layers and onto annealed Ti foils using TFS 200 ALD reactor (Beneq) provided with stop-flow configuration. Palladium(II)hexafluoroacetylacetonate $Pd(C_5HF_6O_2)_2$ (95%, Strem Chemicals) and formalin (37% formaldehyde in water with 10–15% of methanol, Sigma-Aldrich) were used as the Pd precursor and co-reactant, respectively. Pd precursor was heated up to 65°C, while the deposition process temperature was 200°C. One ALD cycle ($N_{ALD} = 1$) was defined by the following sequence: Pd pulse (2 s)-exposure (10 s)-N_2 purge (20 s)-formalin pulse (1 s)-exposure (10 s)-N_2 purge (20 s). A preliminary step to enhance the density of hydroxyl functional groups on the surface substrate was applied to improve the Pd nucleation. Such preliminary step consisted of 5 ALD cycles (water pulse (0.5 s)-exposure (10 s)-N_2 purge (20 s)) followed by 20 cycles (Pd (0.25 s)-exposure (10 s)-N_2 purge (20 s)) was employed with pulse, exposure, and purge durations programmed as "5 * (0.5:10:20 s) and 20 * (0.25:10:20 s)" for H_2O and Pd precursor respectively prior to the actual deposition of Pd. The sole necessity of H_2O pulse is to create -OH functional groups on the substrate so that Pd can nucleate efficiently.

2.3. Characterization methods

Blank and Pd decorated TNTs (Pd/TNTs) and Pd/Ti foils were characterized by scanning electron microscope (SEM) FEI Verios 460L. Pd/TNTs were also characterized bya high-resolution transmission electron microscope (HRTEM) Thermo Fisher Scientific Titan Themis 60-300, operated at 300 kV and equipped with a C_s image aberration corrector, a high angle annular dark field detector for scanning transmission electron microscopy (STEM-HAADF) imaging, and Super-X energy dispersive X-ray (EDX) spectrometer with four 30 mm^2 windowless detectors for STEM-EDX analysis to check the morphology and Pd NPs size/distribution. The crystalline structure of Pd/TNT layers was assessed using X-ray diffraction XRD (Rigaku Smartlab 3 kW diffractometer equipped with Cu-Kα1 radiation source). Surface chemical state of Pd NPs before and after electrochemical measurements were studied using X-ray photoelectron spectroscopy (XPS) Kratos Analytical Axis Supra instrument, with Al-Kα monochromatic X ray source ($h\nu$ = 1486.69 eV). The spectra were deconvoluted using CasaXPS software and referenced to the Femi Level cut off, which means at 0 eV on the binding energy scale. Pd 3d spectra were deconvoluted with asymmetric Lorentzian function LA (1.5, 4, 45) for metallic state (Pd^0), mixed Gaussian-Lorentzian functions GL (30) for Pd oxides or hydroxides and Pd plasmon loss.

2.4. Electrochemical analysis

The electrochemical measurements were carried out in a normal three electrodes electrochemical cell at room temperature. Autolab VIONIC potentiostat supported by INTELLO software was used for this purpose. Two solutions of 1M KOH and 1M KOH/CH_3OH were used as electrolytes. The reference electrode was Ag/AgCl 3M KCl ($E^* = 0.210$ V vs RHE). A Pt foil was used as counter electrode, where Pd decorated Ti

foils (Pd/Ti) and Pd/TNT layers were used as working electrodes. Before every measurement, degassing of all electrolytes was carried out by bubbling with ultra-high purity nitrogen for at least 15 minutes, this to ensure the removal of the dissolved unwanted oxygen that can interfere during the electrochemical oxidation process. All potentials given in this paper were recalculated versus RHE. Cyclic voltammetric (CV) measurements were carried at a scanning rate of 10 mV s^{-1}. Electrochemical impedance spectroscopy (EIS) was conducted using the same setup as above, using methanolic KOH as a solution at 0.8 V vs. RHE. In order to check and compare the stability of various Pd/TNT layers and Pd/Ti foils, chronoamperometric (CA) measurements were performed at an applied potential of 0.9 V vs RHE for 2 hours. The geometrical surface area (0.636 cm^2) was used to determine the current densities. In addition, the electrochemical active surface area (ECSA) has been determined and compared with the literature results.

3. Results and discussion

Fig. 1 shows SEM top-view images of TNT layers (5 μm thick and with an inner diameter of ≈ 250 nm) decorated with Pd NPs using different

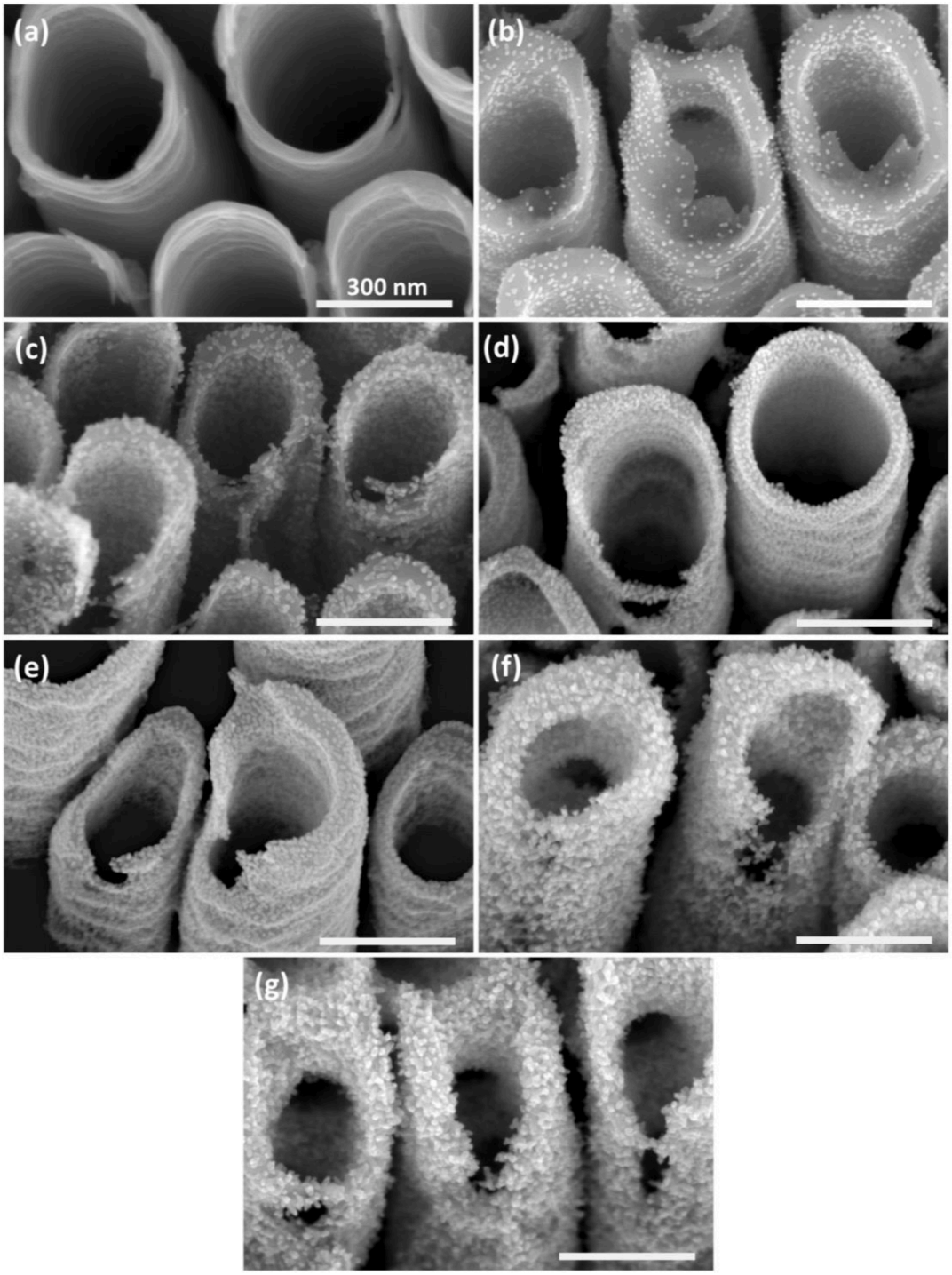

Figure 1. SEM top views of 5 μm thick TNT layers decorated with Pd NPs using different N_{ALD}: (a) 0, (b) 150, (c) 300, (d) 350, (e) 400, (f) 450, (g) 600. The scale bars in all images represent 300 nm.

number of Pd ALD cycles (N_{ALD}): 0, 150, 300, 350, 400, 450 and 600. Homogenous distribution of Pd NPs all along the inner and outer TNT walls was verified. As one can expect, an increase in the N_{ALD} results in a higher density of Pd NPs on the TNT layer surface. From $N_{ALD} \geq 450$ cycles (Fig. 1d), Pd NPs start to coalesce resulting into a porous Pd layer.

Figure S1 shows SEM top-view images of Ti foils decorated with Pd NPs using different number of Pd ALD cycles (N_{ALD}): 0, 150, 300, 350, 400, 450 and 600. The Pd NPs are already coalesced at 300c, which is much earlier than for the TNT layers, which offer slightly different nucleation density and much higher surface area to host higher loading of Pd. Considering the coalescence, the analyses of NPs size from Pd/Ti has no or limited sense. Moreover, TEM analysis of these specimens is not possible, as they are too thick for electrons to pass through.

Corresponding EDX analyses for Pd/TNTs provided the weight percentage (wt %) distribution of C, Ti, O, and Pd. Figure S2 shows an increase in Pd content on Pd/TNT layers with increasing N_{ALD}. EDX spectra shown in Figure S3 approve the increasing Pd along with increasing N_{ALD}.

The morphological features of Pd/TNT layers were further characterized by HRTEM and compared with the non-decorated Pd layer (0 N_{ALD}). TEM images in Fig. 2 provide an overview of high-resolution images showing the size and distribution of Pd NPs on TNTs. The Pd

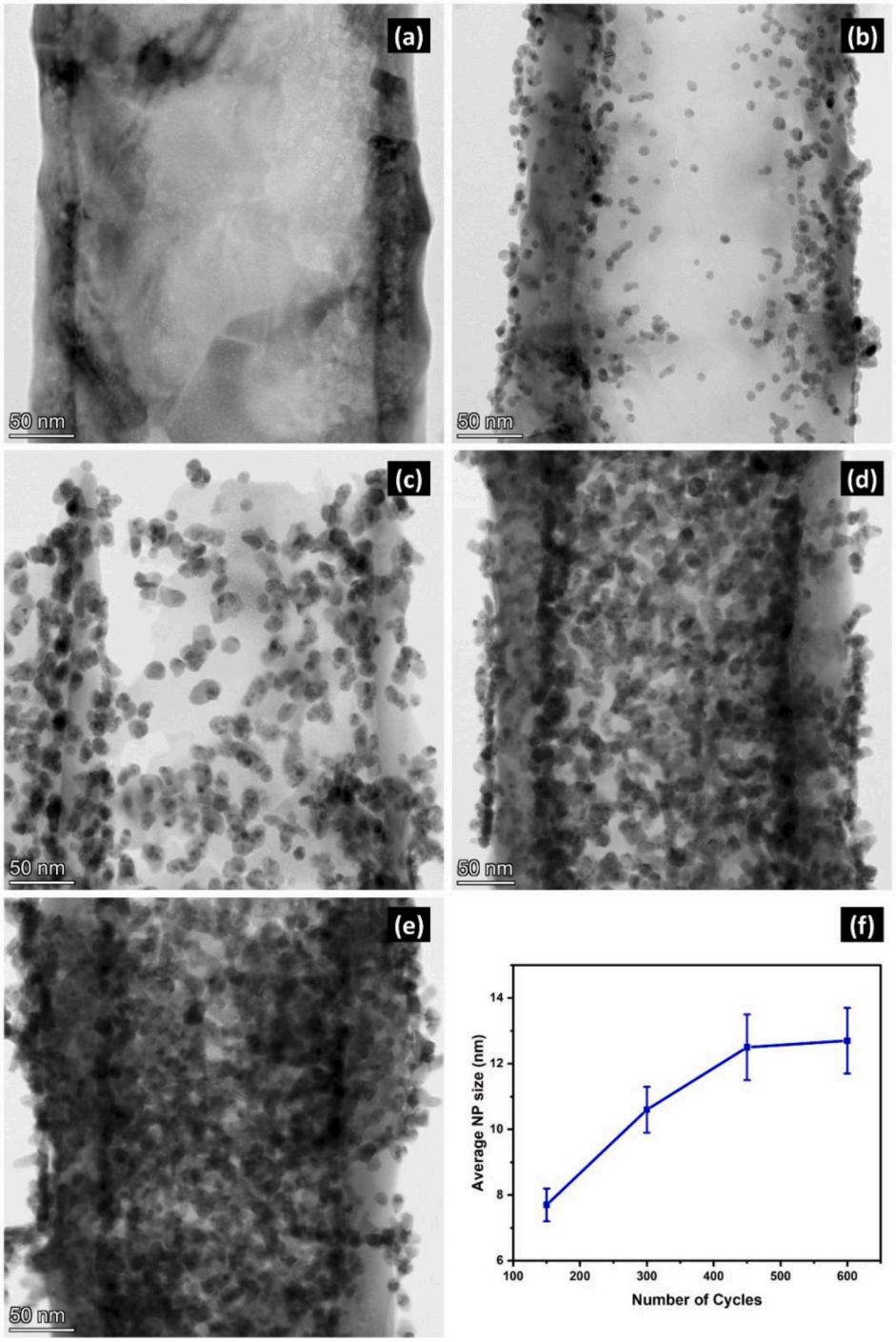

Figure 2. TEM images of single TNT with Pd NPs grown after 0 (a), 150 (b), 300 (c), 450 (d), and 600 (e) Pd N_{ALD}, respectively. (f) Average NPs size as function of N_{ALD} (for the same samples as in a) to e)).

NPs were uniformly distributed all along the walls of TNT layers. As mentioned above, Pd NPs coalescence started from 450 ALD cycles (Fig. 2d). Regarding the Pd NPs size dependency with the number of ALD cycles, Fig. 2f shows the average Pd NPs size for each sample with different number of ALD cycles, determined using the statistical analyses from TEM images. Average Pd NPs sizes for 150, 300, and 450 ALD cycles were 7.5, 10.5, and 12.5 nm respectively. A higher N_{ALD} (600) rendered the coalescence of Pd NPs, thus initiating the process to form a porous Pd layer along the TNT walls.

XRD patterns of the blank TNT layer in Fig. 3a show typical peaks of anatase TiO_2 phase with the major peaks located at 25.2° and 48° representing (101) and (200) anatase peaks. The additional peaks observed at 38.4° and 40.2° represent the (002) and (101) crystalline planes of Ti substrate. The (111) Pd plane diffraction peak observed for higher Pd decorated TNTs (450 and 600 N_{ALD}) should appear at 40.1° but due to overlapping with Ti (101) peak it is difficult to discern. Having a closer look at 600 N_{ALD} 40.1° peak, the peak becomes broader (compared to other peaks) with a lower intensity covering both 40.1° and 40.2°, this is due to the decreasing size of Pd NPs crystals. A broad peak detected around 46.2° could be ascribed as Pd (200), which was visible only in TNT layers decorated with 450 and 600 Pd N_{ALD}. This could be due to formation of porous Pd structure unlike the samples deposited with a lower N_{ALD} (150 and 300) revealing more dispersed Pd NPs within TNT walls, preventing X-ray diffraction detection.

Fig. 3b show high resolution Pd, Pd 3d XPS spectra obtained before and after the CA. Both spectra show the corresponding spin-orbit splitting Pd $3d_{5/2}$ / Pd $3d_{3/2}$ with similar shapes. Seven components were used to deconvolute both spectra; six associated to the spin-orbit splitting, which correspond to three different chemical species, and the leftover for the characteristic plasmon loss that appears as Pd is mostly metallic. The first doublet (red peaks) are centered at 335.3 / 340.6 eV confirming the presence of metallic Pd (Pd^0) [25]. The binding energies corresponding to the second doublet (blue peaks) at 336.9 / 340.5 eV, were related to Pd^{2+} [26], while those from the third doublet (green peaks), located at 338.7 / 344.0 eV were assigned to Pd^{4+} [27]. Pd^{2+} and Pd^{4+} could be related to corresponding oxides or hydroxides [28,29]. Since no major differences were found from chemical species and/or binding energies shifts in Pd spectra before and after the electrochemical measurements, quantification of the oxidation states was performed, as shown in Fig. 3c. According to these results, it is evident that after CA measurements the amount of metallic Pd decreases slightly (around 4.3%), while the content of Pd^{2+} increases.

The surface chemical state of TNT layers decorated with 600 Pd N_{ALD} was investigated before and after the electrochemical measurements by XPS. The survey spectra (Figure S4a) in both cases reveal the presence of C, O, Ti, F and Pd. The C signal comes from the adventitious carbon. The presence of oxygen can be identified from the Auger O KLL signal, since the O 1s has a strong overlapping with the Pd $3p_{3/2}$ signal. Ti peaks are due to the substrate (TNT layers), while F is a remnant from the Ti foil anodization process. In order to verify the chemical nature of TiO_2 after the ALD process, additional high resolution XPS analysis was conducted for Pd/TNTs sample produced with 600c of Pd ALD process (i.e. before any electrochemical experiment). This sample spent the longest time in the ALD reductive atmosphere. Figure S4b shows Ti 2p high resolution spectrum of the corresponding sample. The spectrum reveals only the Ti^{4+} state, since Ti 2p3/2 is at ~459 eV. Thus, it is clear that no reduction of Ti^{4+} to Ti^{3+} occurred during the ALD process.

Fig. 4a exhibits the electrocatalytic activity profile of Pd/Ti foils in electrolyte of 1 M KOH solution. The blank foil shows no response along the CV in the potential range (0 to 1.2 V), indicating no oxidation reaction occurs. Increasing Pd N_{ALD} from 150 to 600 enhanced the current density at lower potentials, showing sharp peak at around 0.1 V. This peak represents the desorption of H on the Pd NPs surface due to the electrolyte (1M KOH) enriched with dissociated hydroxyl groups. While it is well known that the Pd surface gets gradually oxidized as the anodic scan moves towards higher potential region for E > 0.7 V [30], the reverse scan shows a reduction peak at around 0.7 V representing the desorption of oxygen (reduction of PdO to Pd), adsorbed during the previous forward scan between 0.75 and 1.2 V. Fig. 4b depicts the CVs obtained from the set of Pd/Ti foils tested in 1 M KOH/CH_3OH.

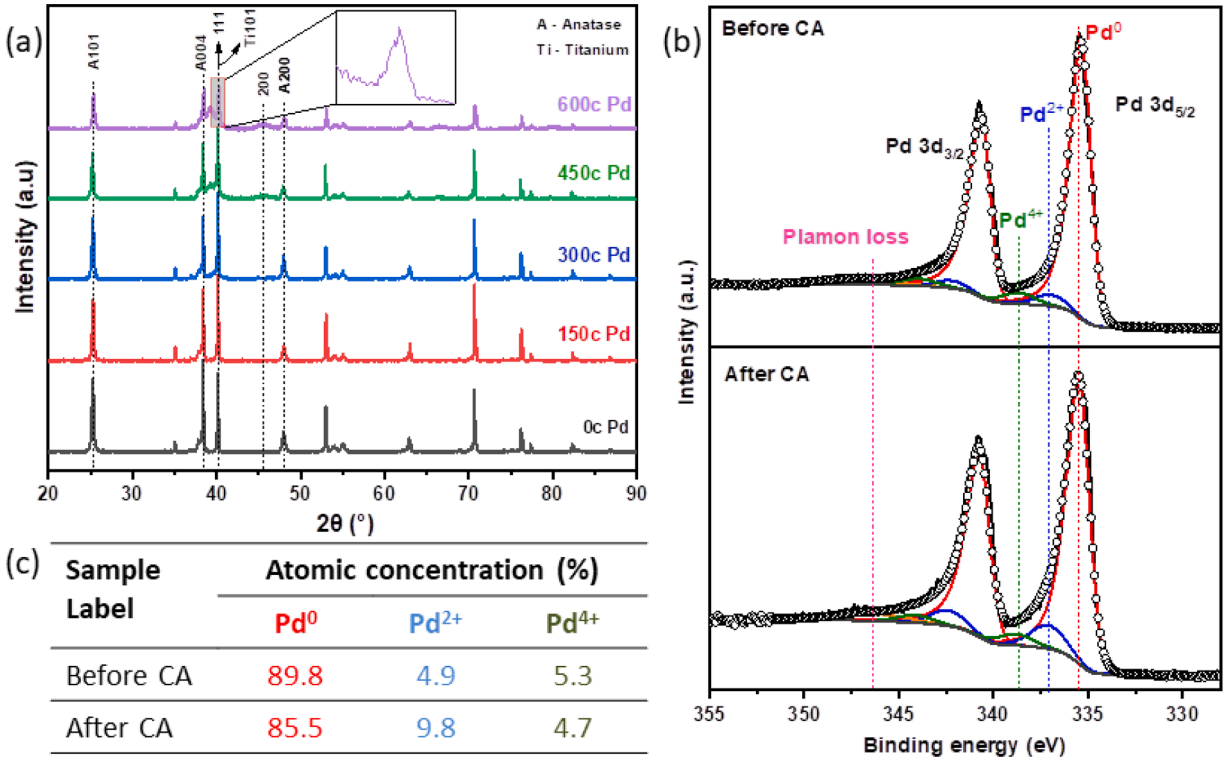

(c)

Sample Label	Atomic concentration (%)		
	Pd^0	Pd^{2+}	Pd^{4+}
Before CA	89.8	4.9	5.3
After CA	85.5	9.8	4.7

Figure 3. (a) XRD patterns of 5 μm thick Pd/TNT layers decorated with N_{ALD} = 0, 150, 300, 450, and 600 Pd. b) Pd 3d XPS high resolution spectra of 600c Pd/TNT layers before and after chronoamperometric (CA) measurements. c) Atomic concentration of Pd deduced by XPS.

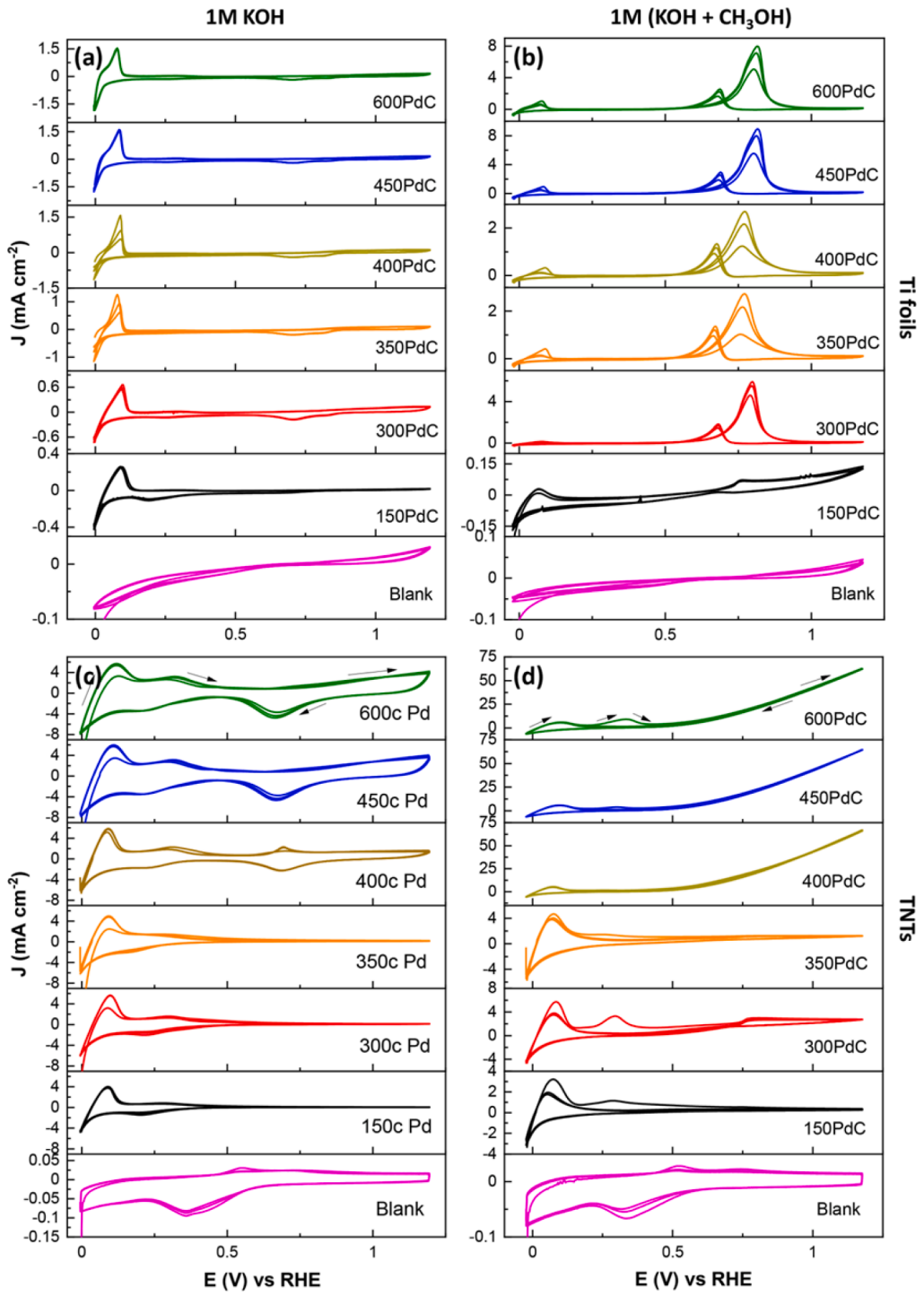

Figure 4. CVs showing three consecutive cycles for Pd/Ti foils (a, b) and Pd/TNT layers (c, d) decorated with different N_{ALD} (0, 150, 300, 350, 400, 450, and 600), recorded in 1 M KOH (a, c) and methanolic (1 M KOH + 1 M CH_3OH) electrolyte by applying a scanning rate of 10 mV s^{-1}.

Noticeable oxidation peaks appear starting from Ti foils decorated with 300 Pd N_{ALD}. The results also indicate that increasing Pd N_{ALD} deposited on Ti foils leads to an increase in the methanol oxidation peak current density, and therefore in the cathodic scan the CO oxidation peak current density. The highest current density value of 8.9 mA cm^{-2} corresponds to the Ti foils decorated with 450 Pd N_{ALD}, while those decorated with 300 and 600 Pd N_{ALD} show comparatively lower values of 5.8 and 7.8 mA cm^{-2} at ~0.8 V (noted from the third CV cycle).

The electrocatalytic activity of Pd NPs on Ti foils in methanolic KOH electrolyte shown in Fig. 4b follows the trend of anodic oxidation of MeOH and cathodic oxidation of CO [31]. The obtained CV scans are explained by the fact that during the anodic scan, the sample surface is being activated within a certain potential range, after which it becomes deactivated by oxide species (such as CO), attached on Pd NPs surface preventing further electro-oxidation of methanol. Oxidation reaction initiates at around 0.7 V and the resulting current density increases to reach the electro-oxidation limit at 0.8 V. At this point (0.8 V), the catalytic active sites of Pd NPs surface were poisoned due to adsorption of CO intermediate formed during methanol oxidation, decreasing the current density until the surface is completely inactivated. However,

reactivation of the Pd NPs surface occurs during the reverse cathodic scan within a potential value ranging between 0.7 and 0.6 V, due to oxidation of the adsorbed CO molecules (to CO_2) and reduction of PdO to metallic Pd.

The metallic Pd and Pd hydroxides are responsible for the increase in the current density among samples of Pd/Ti foils. Along the potential increase in the anodic scan the number of neighboring OH groups on Pd also increases. Thus, such increment of OH groups at higher potentials facilitates an additive effect on the removal of the CO molecules, adsorbed during the anodic scan.

Fig. 4c-d shows the electrocatalytic performance obtained from Pd/TNT layers, which behaves differently from Pd/Ti foils, when it comes to methanol oxidation. TNT layers tested in non-methanolic electrolyte (Fig. 4c) show similar peaks compared with Ti foils. In the oxygen adsorption range (0.7 – 1.2 V), Pd-OH, PdO, and/or PdOx could be formed, while a desorption reduction peak is more pronounced in Pd/TNT layer decorated with 400, 450 and 600 Pd N_{ALD} compared with Ti foils due to higher Pd loadings. Furthermore, Fig. 4d shows Pd/TNT layers performance in methanolic KOH, showing current densities of 66.7, 64.8 and 62.6 mA cm^{-2} obtained at 1.2 V for 400, 450 and 600 Pd N_{ALD} respectively. The CVs show no visible anodic and cathodic peaks, thus representing a featureless polarization curve with an onset potential of 0.5 V. The TNT layer is an oxyphilic oxygen atoms provider. It appears to be an effective oxidizer to mitigate electro-oxidation of methanol on the Pd/TNT layer surface, circumventing either CO poisoning of Pd NPs surface or avoiding formation of intermediate organic species. [8,23,32]

During the electrode deactivation, observed for Pd/Ti foils, CO species, in addition to other intermediates formed during the process of methanol electro-oxidation, are believed to be the main electrode poisoning species. As a matter of fact, based on the previous literature [33] CO is not the only source of poisoning the catalyst surface, and removal of CO is a diffusion controlled process, which explains the slow desorption process. The oxidation of CO_{ads} is considered as the rate determining step according to the following reaction, and it is well known that the complete MOR can yield CO_2 as end product:

$$CH_3OH_{ads} + 4OH^- \rightarrow CO_{ads} + 4H_2O + 4e^- \quad \text{(Eq. 1)}$$

$$CO_{ads} + 2OH^- \rightarrow CO_2 + H_2O + 2e^- \quad \text{(Eq. 2)}$$

In a typical anodic scan of MOR (Fig. 4b) the oxidation starts and carries on until a certain potential where the adsorbed OH groups can no longer react with the available CO molecules adsorbed on the surface (CO_{ads}), leading to a current density drop. CO and OH groups are believed to be evolving during the same potential window. However, the effect of higher potential excels the activity of OH groups. To simplify, CO bonding on the surface can only lead to a loss of surface activity as explained before and shown in (Fig. 4b), while the CO oxidation reaction occurring with the neighboring OH groups, bonded into the surface of high surface area TNTs, plays an important role in clearing CO molecules and the other adsorbed species.

The obtained featureless curves (Fig. 4d) show no decline in the current density during consecutive CVs within the applied potential range (0 to 1.2 V). In order to study such effect, the potential range is split into two parts. A lower potential region below the peak potential value around 0.8 V (Fig. 4b), and a higher region above this value. At the lower potential region, adsorption of methanol takes place, and Eq. (1) applies resulting in CO adsorbed on the surface. Following, Eq. (2) applies at higher potential, supported by the oxophilic nature of TiO_2 and its electron donor properties, which enhance the CO_{ads} oxidation kinetics enough to keep the CH_3OH oxidation without surface blockage by intermediates. Thus, CO_{ads} oxidation reaction is not considered as the rate determining step anymore with the Pd/TNT layers.

The electrochemical surface area (ECSA) was determined using the integrated reduction peak of PdO. The value of charge for the reduction of a PdO monolayer was taken from the literature [34,35] with Q_M = 424 $\mu C/cm^2$. The ECSA value was determined using the following formula.

$$ECSA = \frac{Q_{int}}{Q_M}$$

Since the value of Q_{int} is scan rate dependent, it is correct to use different scan rates for determining the final value of charge integrated from the reduction peak.

The ECSA of Pd/TNT layers decorated with 450 Pd and 600 Pd N_{ALD} were calculated to be 176 cm^2 and 213 cm^2, far higher as compared to 0.636 cm^2 obtained as the corresponding geometrical area (defined as the dimensional area exposed to the electrolyte, without taking the surface porosity into consideration). The ECSA value obtained for the TNT layer decorated with 600 Pd N_{ALD} is about 7 times larger than the ECSA values reported in the literature, which were estimated to be 22.3, 29.6, and 7.1 cm^2 for Pd/TNT layers (500, 700, and 900 Pd N_{ALD}) [2], and 14.2 cm^2 for palladium supported TiO_2 nanotube array (Pd-TNTA) developed by electrochemical milling and faceting (ECMF) method [17].

Electrochemical impedance spectroscopy (EIS) was used as a powerful tool to study the electron-transfer kinetics of the methanol oxidation reaction. EIS measurements were carried out at a frequency range (10^{-2} and 10^5 Hz), and an AC amplitude of 10 mV at a potential of 0.8 V vs RHE in 1M KOH/CH_3OH electrolyte. In general, the charge transfer resistance value is represented by the diameter of the semicircle. A smaller diameter corresponds to a smaller charge transfer resistance, which in turn represents a high charge transfer rate provided the evaluation performed for all the samples at the same potential. Fig. 5 represents the Nyquist plots for Pd/TNT layers decorated with different N_{ALD} of Pd. The Nyquist plots for Ti foils and a comparative assessment of charge transfer resistance values for both foils and TNTs with Pd are provided in Figs. S5 and S6. The decrease in charge transfer resistance for TNTs decorated with N_{ALD} Pd is evident and no significant difference among samples with 400, 450 and 600 N_{ALD} was observed, which aligns with observed current densities from CV for the samples.

In order to evaluate the stability of Pd NPs in 1M KOH electrolyte within the potential range of 0 – 1.4V, 22 consecutive CV cycles were performed for TNTs decorated with Pd NPs using N_{ALD} = 600, as shown in Fig. 6. The resulting CV curves showed several meaningful regions in the anodic as well as in the cathodic scan, as described ahead. The lower potential region (1) corresponds to hydrogen desorption or adsorption in addition to K^+ cation species [36]. This process takes place as a result of a previous adsorption process happened during the reverse scan at potential ranges between (0 – 0.2V). The peak intensity increase with cycling could be due to accumulation of the adsorbed species at the surface during cycling. In region (2), the lower current density corresponds to the double layer charge, but the current density increases upon cycling. It is shown in ref. [37] that it is unlikely that the rise of the anodic peak during cycling is related to oxide formation. At the same time, the decrease in oxygen adsorption current density (region 3) may indicate the lower quantities of the adsorbed OH groups on the surface and PdO could be formed alternatively. The detailed oxidation process is not yet fully understood. The formed OH groups react with monoxides obtained during dehydrogenation process leading to a complete reaction. Then the slight increase in current density of the sharp cathodic peak (region 4) represents the reduction of PdO into Pd, where the intensity increases with increasing the palladium oxide on surface.

In order to exploit the stability of Pd NPs on TNTs in 1M KOH + 1M CH_3OH electrolyte, 22 consecutive CV cycles were performed for TNTs decorated with Pd NPs using N_{ALD} = 450, within the potential range of 0 – 1.2V. The resulting CV curves shown in Figure S7 prove very good stability of the sample tested.

In order to gain further insight into the stability of the Pd/Ti foils and Pd/TNT layers' electrocatalyst, chronoamperometric (CA) measurements were carried out for 2 hours at 0.9 V. CA curves obtained for Pd/TNT layers are shown in Fig. 7. CA curves for Pd/Ti foils are shown in Figure S8. Pd/Ti foils show a drastic decrease in the current densities

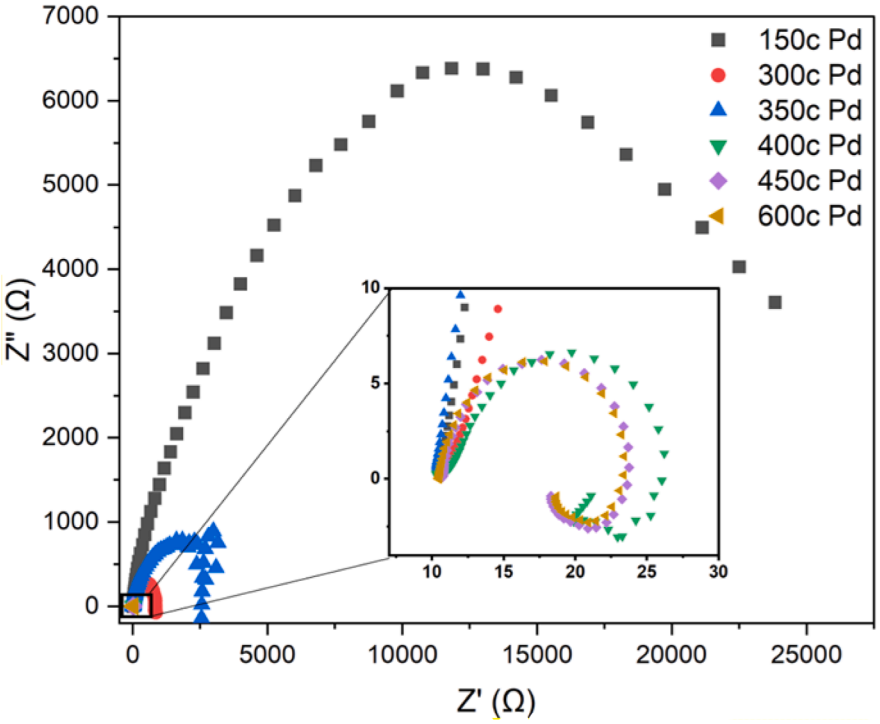

Figure 5. EIS Nyquist plots for Pd/TNT layers in methanolic (1 M KOH + 1 M CH_3OH) electrolyte using different N_{ALD}.

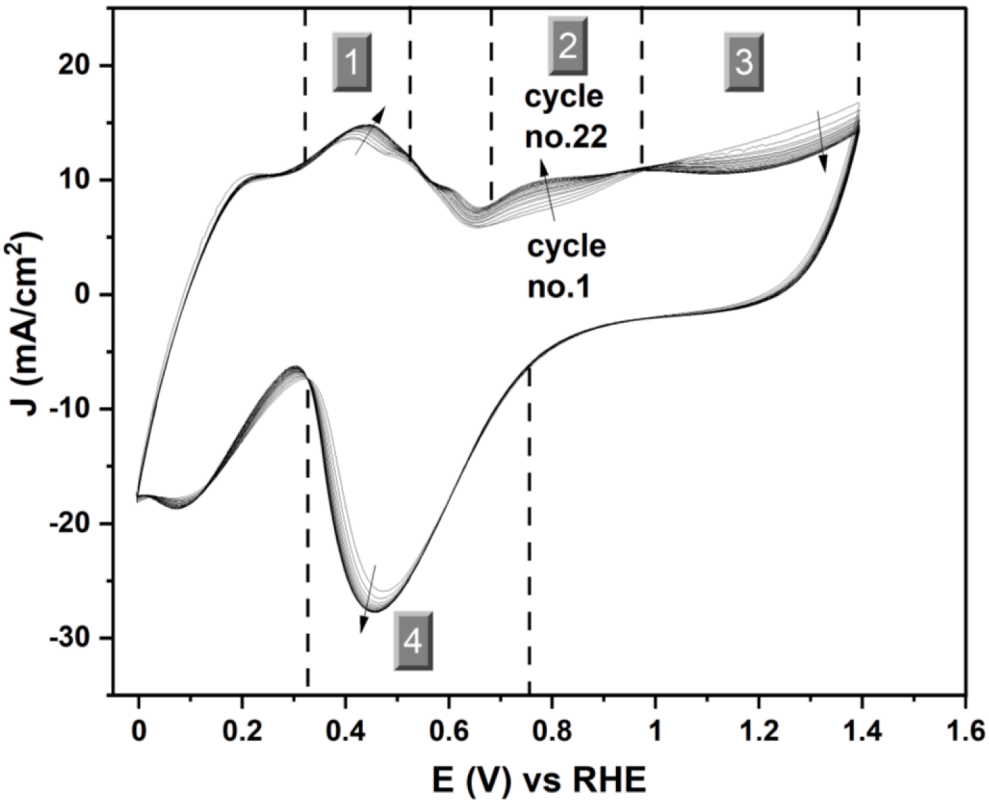

Figure 6. CV curves (22 consecutive cycles) obtained in 1M KOH for 5μm TNTs decorated with Pd NPs using N_{ALD} = 600.

during the CA analysis confirming the effect of CO poisoning that led to a loss of active sites responsible for methanol electro-oxidation. Whereas the results obtained from Pd/TNT layers confirm the benefits of noble metal - metal oxide support interaction, by providing significantly higher tolerance to CO poisoning. The CA results depict relatively stable current densities along the CA test for the Pd/TNT layers decorated with 600 Pd N_{ALD}, developing a current density of 28.5 mA cm^{-2} (Fig. 7). In contrast, the Pd/TNT layers decorated with 450, 400, 350, 300, and 150

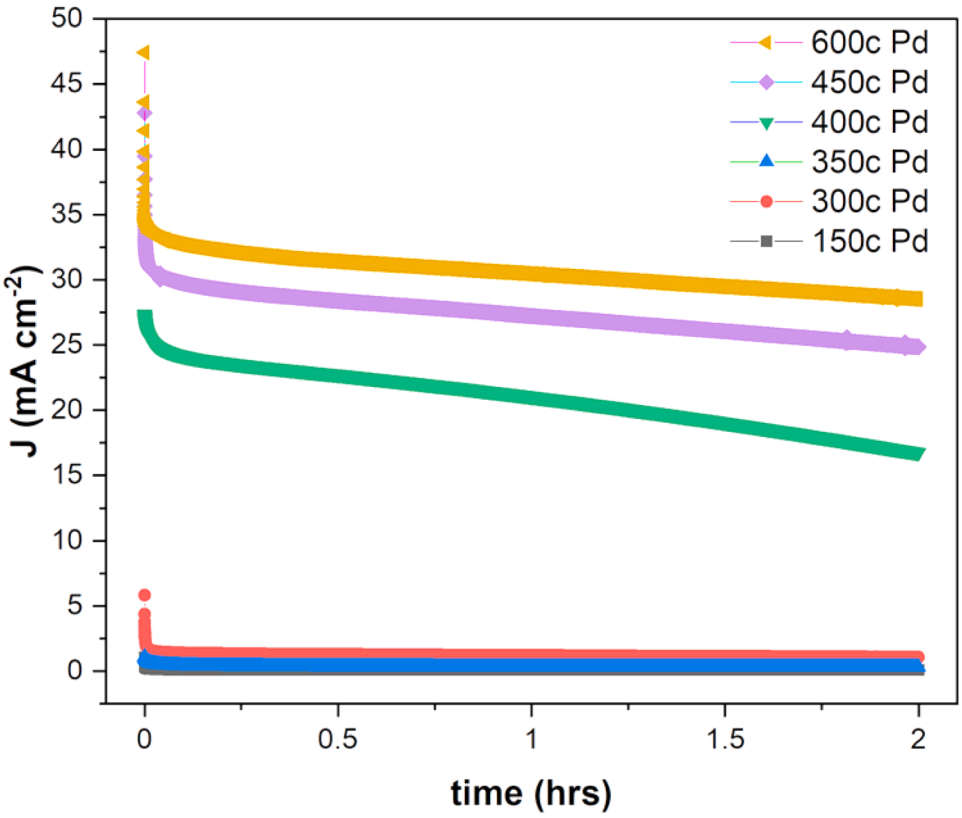

Figure 7. Chronoamperometric (CA) curves demonstrating the stability of Pd/TNT layers with different N_{ALD} (150, 300, 350, 400, 450, and 600). CA curves were recorded in 1M KOH + 1M CH_3OH at $0.9V_{RHE}$ for 2 h.

Pd N_{ALD} show comparatively a higher current density drop (compared to the initial current density) after 2h test, with current densities of 24.8, 16.7, 0.5, 1.07, and 0.07 mA cm^{-2}, respectively. Interestingly, the drop in current densities was attenuated for a higher Pd N_{ALD}. Thus, the percentages of current density loss were 16.1%, 23.7%, 32.1%, 42.8%, 49%, and 75.8% for 600, 450, 400, 350, 300 and 150Pd N_{ALD}, respectively. Therefore, the results indicate that the Pd NPs size plays a significant role in the electrocatalytic performance. Thus, the dominance of the OH coverage on small Pd NPs will decrease the catalytic active Pd surface responsible for methanol adsorption, leading to a higher drop in the current densities under long term performance [38]. Hence, based on the results obtained in this work, it is suggested that the

Table 1
Overview of current densities obtained from the published literature and compared with density acquired in this work. All values determined or calculated at 0.9V vs RHE, if not denoted otherwise.

		From CV			From CA	
	Substrate	**Scan rate mV. s^{-1}**	**Current density (mA cm^{-2})**	**Onset potential**	**Area considered fromcurrent density (mA cm^{-2}) @time@ V**	**Ref.**
Ethanol oxidation	SnO_2/Pd 500 cycles	25	1.19 ECSA	-0.465	(ECSA) 0.4 @0s 0.19 @3500s	[39]
	TiO_2 TNTs/Pd 500 cycles	25	0.63 ECSA	-0.465	(ECSA) 0.2375 @0s 0.175 @3500s	[2]
	Pd/TiO_2C	50	18	0.424	Chronopotentiometric 3mA/cm^2 @0s@0.57V 3mA/cm^2 @28800s@ 0.72V	[19]
Methanol oxidation	Smooth Pt electrode	50	3.84×10^{-9} A	0.5	NA	[40]
	Pd/C	20	3.1	0.6	NA	[30]
	PdRh/C	20	5	0.6	NA	
	Pd/TiO_2 NTs in H_2SO_4	50	8.66 A	0.436	NA	[41]
	60-65% porous Pd	25	710	0.15	NA	[10]
	Pd/TiO_2-C	50	2.24 (ECSA)	0.44	(ECSA) 1.83 @7200s	[42]
	TiO_2/Pd 450 cycles	10	32	~0.5	(Geometric) 24.8 @7200sec @0.9V	This work

drop in current densities is in relation to the size of Pd NPs deposited onto TNT layers for different N_{ALD}, where the current density stability follows this trend: 600 > 450 > 400 > 350 > 300 > 150c. It is worth clarifying that the current drop in the same plot can be separated into two parts. The fast drop during the first few seconds was followed by constant slow drop with time. As the potential is triggered, the high current recorded just after t = 0 s is due to the trapped electrons at the surface. The later slow current density decrease is ascribed to gradual oxidation of metallic Pd to PdO (Pd^{2+}) as observed in Fig. 3c. In the next period, the current densities are much more stable. In addition to the ability of Pd/TNT layers to stand against poisoning, the obtained current densities show decent records, when compared with other literatures – for comparison see Table 1.

4. Conclusion

ALD is an effective method to load NP of Pd on high aspect ratio substrates. Thus, it was used to decorate TNT layer by Pd NPs using different number of ALD cycles. The mechanism of methanol electrochemical oxidation was successfully assessed using CV and extended potentiostatic measurements. The formation of featureless curves represents an innovation in bypassing the poisoning effects of methanol electro-oxidation intermediates. The advantage of this process can be claimed to the presence of TiO_2, an oxophilic supporting material for Pd NPs, which effectively promote a complete conversion of CH_3OH to CO_2. In addition to the supporting effect of the TiO_2 nanotube substrate, NPs size proved to show an important effect against surface deactivation, where increasing the NPs size from 7.5 to 12.5 nm (towards porous Pd layer) shows a much lower loss in current. Notably, XPS analysis for 600c Pd provided significant evidence about the Pd oxidation state after chronoamperometric measurements, obtained as 85.5% in metallic form of Pd^0, which slightly lower value compared to before CA. Such that, the decrease in metallic Pd content (oxidized to Pd^{2+}) can stand as the main reason of activity loss during methanol electro-oxidation, where no clear poisoningdetected as an effect of adsorbed carbonyl groups on the surface of Pd NPs.

CRediT authorship contribution statement

Bilal Bawab: Conceptualization, Data curation, Formal analysis, Investigation, Methodology, Visualization, Writing – original draft, Writing – review & editing. **Sitaramanjaneya M. Thalluri:** Conceptualization, Data curation, Formal analysis, Investigation, Writing – review & editing. **Jhonatan Rodriguez-Pereira:** Formal analysis, Data curation, Visualization, Writing – review & editing. **Hanna Sopha:** Investigation, Writing – review & editing. **Raul Zazpe:** Conceptualization, Investigation, Methodology, Writing – review & editing. **Jan M. Macak:** Conceptualization, Methodology, Funding acquisition, Project administration, Supervision, Writing – review & editing.

Declaration of competing interest

The authors declare that they have no known competing financial interests or personal relationships that could have appeared to influence the work reported in this paper.

The authors declare the following financial interests/personal relationships which may be considered as potential competing interests:

Data Availability

Data will be made available on request.

Acknowledgments

The authors gratefully acknowledge support from European Union Horizon 2020 program (project HERMES, nr. 952184) and the Ministry of Education, Youth and Sports of the Czech Republic (projects LM2018103 and LM 2018110). Analyses were carried out with the support of CEITEC Nano Research Infrastructure and CEMNAT. We thank MSc. Jan Michalicka and Dr. Eva Kolibalova for HR-TEM analyses.

Supplementary materials

Supplementary material associated with this article can be found, in the online version, at doi:10.1016/j.electacta.2022.141044.

References

[1] V.C. Anitha, R. Zazpe, M. Krbal, J.E. Yoo, H. Sopha, J. Prikryl, G. Cha, S. Slang, P. Schmuki, J.M. Macak, Anodic TiO_2 nanotubes decorated by Pt nanoparticles using ALD: an efficient electrocatalyst for methanol oxidation, J. Catal. 365 (2018) 86–93, https://doi.org/10.1016/j.jcat.2018.06.017.

[2] L. Assaud, N. Brazeau, M.K.S. Barr, M. Hanbücken, S. Ntais, E.A. Baranova, L. Santinacci, Atomic layer deposition of Pd nanoparticles on TiO_2 nanotubes for ethanol electrooxidation: synthesis and electrochemical properties, ACS Appl. Mater. Interfaces 7 (2015) 24533–24542, https://doi.org/10.1021/acsami.5b06056.

[3] S. Kunz, F.F. Schweinberger, V. Habibpour, M. Röttgen, C. Harding, M. Arenz, U. Heiz, Temperature dependent CO oxidation mechanisms on size-selected clusters, J. Phys. Chem. C 114 (2010) 1651–1654, https://doi.org/10.1021/jp911269z.

[4] P. Trogadas, V. Ramani, Pt/C/MnO_2 hybrid electrocatalysts for degradation mitigation in polymer electrolyte fuel cells, J. Power Sources. 174 (2007) 159–163, https://doi.org/10.1016/j.jpowsour.2007.08.088.

[5] D. Horiguchi, T. Tsukatsune, Z. Noda, A. Hayashi, K. Sasaki, Pt/SnO_2 electrocatalysts on conductive fillers, ECS Trans. 64 (2014) 215–220, https://doi.org/10.1149/06403.0215ecst.

[6] M. Xu, P. Da, H. Wu, D. Zhao, G. Zheng, Controlled Sn-doping in TiO_2 nanowire photoanodes with enhanced photoelectrochemical conversion, Nano Lett. 12 (2012) 1503–1508, https://doi.org/10.1021/nl2042968.

[7] A.R. Puigdollers, P. Schlexer, S. Tosoni, G. Pacchioni, Increasing oxide reducibility: the role of metal/oxide interfaces in the formation of oxygen vacancies, ACS Catal. 7 (2017) 6493–6513, https://doi.org/10.1021/acscatal.7b01913.

[8] Y. Suchorski, S.M. Kozlov, I. Bespalov, M. Datler, D. Vogel, Z. Budinska, K. M. Neyman, G. Rupprechter, The role of metal/oxide interfaces for long-range metal particle activation during CO oxidation, Nat. Mater. 17 (2018) 519–522, https://doi.org/10.1038/s41563-018-0080-y.

[9] M. Bellini, E. Berretti, M. Innocenti, G. Magherini, M.V. Pagliaro, L. Poggini, H. A. Miller, A. Lavacchi, F. Vizza, 3D titania nanotube array support for water electrolysis palladium catalysts, Electrochim. Acta 383 (2021), 138338, https://doi.org/10.1016/j.electacta.2021.138338.

[10] R. Manoharan, J. Prabhuram, Possibilities of prevention of formation of poisoning species on direct methanol fuel cell anodes, J. Power Sources. 96 (2001) 220–225, https://doi.org/10.1016/S0378-7753(00)00683-2.

[11] J.L. Cohen, D.J. Volpe, H.D. Abruña, Electrochemical determination of activation energies for methanol oxidation on polycrystalline platinum in acidic and alkaline electrolytes, Phys. Chem. Chem. Phys. 9 (2007) 49–77, https://doi.org/10.1039/b612040g.

[12] S.M. Lang, T. Schnabel, T.M. Bernhardt, Reactions of carbon monoxide with free palladium oxide clusters: strongly size dependent competition between adsorption and combustion, Phys. Chem. Chem. Phys. 14 (2012) 9364–9370, https://doi.org/10.1039/c2cp23976k.

[13] H.X. Zhang, C. Wang, J.Y. Wang, J.J. Zhai, W. Bin Cai, Carbon-supported Pd-Pt nanoalloy with low Pt content and superior catalysis for formic acid electro-oxidation, J. Phys. Chem. C 114 (2010) 6446–6451, https://doi.org/10.1021/jp100835b.

[14] L.M. Palma, T.S. Almeida, A.R. de Andrade, Comparative study of catalyst effect on ethanol electrooxidation in alkaline medium: Pt- and Pd-based catalysts containing Sn and Ru, J. Electroanal. Chem. 878 (2020), 114592, https://doi.org/10.1016/j.jelechem.2020.114592.

[15] M.K.S. Barr, L. Assaud, N. Brazeau, M. Hanbücken, S. Ntais, L. Santinacci, E. A. Baranova, Enhancement of Pd catalytic activity toward ethanol electrooxidation by atomic layer deposition of SnO_2 onto TiO_2 Nanotubes, J. Phys. Chem. C 121 (2017) 17727–17736, https://doi.org/10.1021/acs.jpcc.7b05799.

[16] X. Zhang, J. Zhu, C.S. Tiwary, Z. Ma, H. Huang, J. Zhang, Z. Lu, W. Huang, Y. Wu, Palladium nanoparticles supported on nitrogen and sulfur dual-doped graphene as highly active electrocatalysts for formic acid and methanol oxidation, ACS Appl. Mater. Interfaces 8 (2016) 10858–10865, https://doi.org/10.1021/acsami.6b01580.

[17] Y.X. Chen, A. Lavacchi, S.P. Chen, F. Di Benedetto, M. Bevilacqua, C. Bianchini, P. Fornasiero, M. Innocenti, M. Marelli, W. Oberhauser, S.G. Sun, F. Vizza, Electrochemical milling and faceting: size reduction and catalytic activation of palladium nanoparticles, Angew. Chem. Int. Ed. 51 (2012) 8500–8504, https://doi.org/10.1002/anie.201203589.

[18] W. Xu, S. Zhu, Z. Li, Z. Cui, X. Yang, Synthesis and catalytic properties of Pd nanoparticles loaded nanoporous TiO_2 material, Electrochim. Acta 114 (2013) 35–41, https://doi.org/10.1016/j.electacta.2013.09.084.

[19] F. Hu, F. Ding, S. Song, P.K. Shen, Pd electrocatalyst supported on carbonized TiO_2 nanotube for ethanol oxidation, J. Power Sources 163 (2006) 415–419, https://doi.org/10.1016/j.jpowsour.2006.09.039.
[20] Y.H. Qin, H.H. Yang, R.L. Lv, W.G. Wang, C.W. Wang, TiO_2 nanotube arrays supported Pd nanoparticles for ethanol electrooxidation in alkaline media, Electrochim. Acta 106 (2013) 372–377, https://doi.org/10.1016/j.electacta.2013.05.067.
[21] A. Merenda, M. Weber, M. Bechelany, F.M. Allioux, L. Hyde, L. Kong, L.F. Dumée, Fabrication of Pd-TiO_2 nanotube photoactive junctions via atomic layer deposition for persistent pesticide pollutants degradation, Appl. Surf. Sci. 483 (2019) 219–230, https://doi.org/10.1016/j.apsusc.2019.03.285.
[22] J. Lu, J.G. Bao, X. Lu, D. Zheng, X. Li, Application of a Pd-TiO_2 nanotube/Ti electrode prepared by atomic layer deposition to reductive dechlorination of trichloroethylene, Electrochem. Commun. 103 (2019) 72–76, https://doi.org/10.1016/j.elecom.2019.05.007.
[23] J. Shu, R. Li, Z. Lian, W. Zhang, R. Jin, H. Yang, S. Li, *In-situ* oxidation of Palladium–Iridium nanoalloy anchored on Nitrogen-doped graphene as an efficient catalyst for methanol electrooxidation, J. Colloid Interface Sci. 605 (2022) 44–53, https://doi.org/10.1016/j.jcis.2021.07.056.
[24] S. Das, H. Sopha, M. Krbal, R. Zazpe, V. Podzemna, J. Prikryl, J.M. Macak, Electrochemical infilling of $CuInSe_2$ within TiO_2 nanotube layers and subsequent photoelectrochemical studies, ChemElectroChem 4 (2017) 495–499, https://doi.org/10.1002/celc.201600763.
[25] M.C. Militello, S.J. Simko, Elemental palladium by XPS, Surf. Sci. Spectra 3 (1994) 387–394, https://doi.org/10.1116/1.1247783.
[26] T.L. Barr, Recent advances in x-ray photoelectron spectroscopy studies of oxides, J. Vac. Sci. Technol. A 9 (1991) 1793–1805, https://doi.org/10.1116/1.577464.
[27] D. German, E. Pakrieva, E. Kolobova, S.A.C. Carabineiro, M. Stucchi, A. Villa, L. Prati, N. Bogdanchikova, V. Cortés Corberán, A. Pestryakov, Oxidation of 5-hydroxymethylfurfural on supported Ag, Au, Pd and bimetallic Pd-Au catalysts: effect of the support, Catalysts 11 (2021), https://doi.org/10.3390/catal11010115.
[28] G.A. Shafeev, J.M. Themlin, L. Bellard, W. Marine, A. Cros, Enhanced adherence of area-selective electroless metal plating on insulators, J. Vac. Sci. Technol. A 14 (1996) 319–326, https://doi.org/10.1116/1.579895.
[29] W. Gao, R. Jin, J. Chen, X. Guan, H. Zeng, F. Zhang, Z. Liu, N. Guan, Titania-supported Pd–Cu bimetallic catalyst for the reduction of nitrite ions in drinking water, Catal. Lett. 91 (2003) 25–30, https://doi.org/10.1023/B:CATL.0000006312.32227.4a.
[30] T. Jurzinsky, B. Kintzel, R. Bär, C. Cremers, J. Tübke, Methanol oxidation on PdRh/C electrocatalyst in alkaline media: temperature and methanol concentration dependencies, J. Electroanal. Chem. 776 (2016) 49–52, https://doi.org/10.1016/j.jelechem.2016.06.038.
[31] P. Krawczyk, T. Rozmanowski, M. Frankowski, Methanol electrooxidation at electrodes made of exfoliated graphite/nickel/palladium composite, Catal. Lett. 149 (2019) 2307–2316, https://doi.org/10.1007/s10562-019-02785-9.
[32] W.C. Wu, C.C. Chuang, J.L. Lin, Bonding geometry and reactivity of methoxy and ethoxy groups adsorbed on powdered TiO_2, J. Phys. Chem. B 104 (2000) 8719–8724, https://doi.org/10.1021/jp0017184.
[33] P.S. Deshpande, V.R. Chaudhari, B.L.V. Prasad, Mechanistic aspects of methanol electro-oxidation reaction through cyclic voltammetry: is it correct to blame carbon monoxide for catalyst poisoning? Energy Technol. 8 (2020) 1–7, https://doi.org/10.1002/ente.201900955.
[34] R. Ojani, Z. Abkar, E. Hasheminejad, J.B. Raoof, Rapid fabrication of Cu /Pd nano / micro-particles porous-structured catalyst using hydrogen bubbles dynamic template and their enhanced catalytic performance for formic acid electrooxidation, Int. J. Hydrog. Energy 39 (2014) 7788–7797, https://doi.org/10.1016/j.ijhydene.2014.03.081.
[35] S. Li, M. Yang, R. Jin, H. Niu, C. Liao, H. Yang, J. Jin, J. Ma, Coupling palladium nanocrystals over D-phenylalanine-functionalized carbon nanotubes as an advanced electrocatalyst for hydrogen evolution and ethanol oxidation, Electrochim. Acta 364 (2020), 137290, https://doi.org/10.1016/j.electacta.2020.137290.
[36] T.E. Society, C. Augusto, C. Rold, Experimental protocol for HOR and ORR in alkaline electrochemical measurements Jes F Ocus I Ssue On E Lectrocatalysis — I N H Onor Of R Adoslav A Dzic Experimental Protocol for HOR and ORR in Alkaline, J. Electrochem. Soc. 165 (2018), J3001, https://doi.org/10.1149/2.0011815jes.
[37] D. Zhan, J. Velmurugan, M.V. Mirkin, Adsorption /desorption of hydrogen on Pt nanoelectrodes : evidence of surface diffusion and spillover, J. Am. Chem. Soc. 131 (41) (2009) 14756–14760, https://doi.org/10.1021/ja902876v.
[38] D.Y. Chung, K.J. Lee, Y.E. Sung, Methanol electro-oxidation on the Pt surface: revisiting the cyclic voltammetry interpretation, J. Phys. Chem. C 120 (2016) 9028–9035, https://doi.org/10.1021/acs.jpcc.5b12303.
[39] M.K.S. Barr, L. Assaud, N. Brazeau, M. Hanbücken, S. Ntais, L. Santinacci, E. A. Baranova, Enhancement of Pd catalytic activity toward ethanol electrooxidation by atomic layer deposition of SnO_2 onto TiO_2 nanotubes, J. Phys. Chem. C 121 (2017) 17727–17736, https://doi.org/10.1021/acs.jpcc.7b05799.
[40] E.D. Rus, R.H. Wakabayashi, H. Wang, H.D. Abruña, Methanol oxidation at platinum in alkaline media: a study of the effects of hydroxide concentration and of mass transport, ChemPhysChem (2021), https://doi.org/10.1002/cphc.202100087.
[41] M. Wang, D.J. Guo, H.L. Li, High activity of novel Pd/TiO_2 nanotube catalysts for methanol electro-oxidation, J. Solid State Chem. 178 (2005) 1996–2000, https://doi.org/10.1016/j.jssc.2005.04.006.
[42] R. Liang, A. Hu, J. Persic, Y.N. Zhou, Palladium nanoparticles loaded on carbon modified TiO_2 nanobelts for enhanced methanol electrooxidation, Nano Micro Lett. 5 (2013) 202–212, https://doi.org/10.1007/bf03353751.